Induction, helicity, and alpha effect in a toroidal screw flow of liquid gallium

R. Stepanov,[1] R. Volk,[2] S. Denisov,[1] P. Frick,[2] V. Noskov,[1] and J.-F. Pinton[2]
[1]*Institute of Continuous Media MechanicsKorolyov 1, 614061 Perm, Russia*
[2]*Laboratoire de Physique de l'Ecole Normale Superieur de Lyon,, CNRS UMR5672, 46 allee d'Italie, 69007 Lyon, France*
(Received 19 December 2005; published 27 April 2006)

We investigate experimentally induction mechanisms in a screw flow of gallium in a toroidal channel. The flow is nonstationary and operated in a spin-down regime: the channel (and fluid) are initially set into solid body rotation; as the channel is stopped the fluid is set into strong helical motion by diverters located inside the channel. In this study, we put a particular emphasis on the induction generated by these helical motions, which are expected to develop over the entire range of turbulent scales. We apply an external magnetic field either perpendicular to the channel axis parallel to it. At large scales the nonlinear induction mechanisms are associated with the Parker stretch and twist effect and with the expulsion due to overall rotation. Induction mechanisms can also originate in the small scale helicity as in the alpha induction effect of mean-field magnetohydrodynamics. Our measurements yield an upper bound for the alpha coefficient, significantly lower than estimates based on dimensional analysis. We discuss the consequences of our observations for the engineering of homogeneous dynamos in the laboratory.

DOI: 10.1103/PhysRevE.73.046310 PACS number(s): 47.65.−d, 52.65.Kj, 91.25.Cw

I. MOTIVATION

The study of magnetic induction by the motion of electrically conducting fluids has received much attention in a wide variety of communities ranging from the metallurgy industry, power companies (magnetic storms, sodium flows in cooling circuits of breeder reactors) and, of course, the physics, astrophysics, and geophysics communities. When the fluid is in motion, the electrical currents induced are given by Ohm's law

$$\mathbf{j} = \sigma(\mathbf{B} + \mathbf{u} \times \mathbf{B}), \tag{1}$$

where σ is the conductivity, $\mathbf{u}$ the velocity, and $\mathbf{B}$ is the total magnetic field (sum of the applied field $\mathbf{B}_0$ and induced field $\mathbf{B}^I$). In the treatment of the induction due to the fluid motion, one situation of particular interest concerns situations in which the flow responds to an externally applied field by the generation of an induced electrical current parallel to the applied field $\mathbf{j}=\alpha(\mathbf{u})\mathbf{B}_0$. In this expression α is a function which depends on the properties of the flow, and has the physical dimension of a velocity. The interest of having such an induced current is that it generates a magnetic field $\mathbf{B}^I$ perpendicular to $\mathbf{B}_0$. This feature is often used in the modeling of induction and of the dynamo effect in planets and stars [1–5]. It has been measured experimentally in constrained [6,7] and homogeneous flows of liquid sodium [8,9] and it governs the Karlsruhe dynamo [10,11]. Parker has proposed a mechanism [12], from purely geometrical considerations, as a stretch and twist of the applied field by helical motion. Note that this Parker effect relies on the topology of the fluid motion and does not imply small scale turbulence. In the context of homogeneous turbulence, an equation $\mathbf{j}=\alpha(\mathbf{u})\mathbf{B}$ has derived in the framework of mean-field magnetohydrodynamics [13]—in general the above relationship should be expressed in tensorial form; we will return to this point later, but we emphasize that we focus on the generation of an effective electromotive force in the direction of the applied field. In the mean-field approach, one assumes a scale separation in the flow, and the current $\mathbf{j}$ results from the mean electromotive force produced by induction at small scales. It is a collective, small scale effect, usually referred to as the alpha effect. Although the alpha effect is very often invoked in models of geo or astro dynamos [3,5], it has not been experimentally measured yet in unconstrained turbulent flows. Note that there are not well-defined boundary between the Parker effect and the alpha effect (for instance the Karlsruhe flow can be viewed as both). We imply hereafter that the alpha effect is intrinsically based on chaotic (turbulent) flows, while the term "Parker effect" is attributed to the similar action of regular helical flows.

This paper reports measurements in a gallium screw flow in a toroidal channel, the Perm experiment [14], which has the property of a large injection of helicity in the large scales. The flow is of the spin-down type. It is generated by the sudden halt of a fast rotating torus field with gallium—experimental details are given in the next section, we focus here on its main features. As the vessel stops, the fluid is set into helical motion as it crosses a bladed diverter. Even though the resulting flow is decaying in time, the kinetic Reynolds numbers reached are very large (of the order of 10^6), so that the fluid motion extends over a large range of scales. Initially, a large kinetic helicity is imparted to the flow, at a scale of the order of the torus diameter. Integrated kinetic helicity is conserved in inviscid fluid motion and when viscosity is taken into account, one expects a helicity cascade to the small scales. This has been shown in several numerical simulations [15], although not yet evidenced experimentally due to the difficulty of performing local measurements of helicity. One thus expects that the flow in the torus has helicity on a broad range of scales, from the integral length (of the order of the torus diameter) to the dissipative scale of turbulence. This is an interesting prospect because helicity is intimately linked to the Parker and alpha effects [16]. A large scale screw motion generates a Parker effect [9]; its amplitude varies quadratically with the integral

Reynolds number and its sign is opposite to that of the flow helicity. When helicity is distributed at small scales, mean-field hydrodynamics calculations show how an alpha effect can be generated. For instance, an array of small-scale helical motion can act as an alpha generator. This happens in the analytical Roberts flow, for which the dynamo capacity was demonstrated in the Karlsruhe experiment. Note that the distribution of like-sign helicity in the Karlsruhe experiment is enforced by the walls of the inner channels. The distribution of helicity will be different in a homogeneous flow, and the consequences regarding alpha generation can be drastic. For instance, it can be shown that no alpha effect is possible in a parity invariant flow. As a result, alpha generation is absent from homogeneous, isotropic turbulence—this is no longer the case if the turbulence is stratified. In the Perm screw flow, helicity is expected to be distributed across all scales of motion, so that it can be *a priori* considered as a candidate for both Parker and alpha effects.

In the study reported here, we report experimental measurements in the Perm flow of liquid gallium. An external magnetic field is applied on the flow, and ideally one would like to probe directly the $\mathbf{j}=\alpha(\mathbf{u})\mathbf{B}_0$ relationship. This is not possible because current measurements are difficult, and we perform instead magnetic induction measurements either locally with magnetic probes or globally using induction coils. In a complex homogenous flow, many velocity gradients contribute to the induction and one should be able to discriminate. Hence, particular attention will be paid to the symmetries of the induction measurements. They have proven to be particularly useful in the identification of induction effects [9,17,18].

II. FLOW AND MEASUREMENTS

We describe in this section the hydrodynamics characteristics of the screw flow and our measurement methods.

A. The Perm screw flow

A schematic diagram of the gallium set up is given in Fig. 1. The set up consists of a toroidal channel (1) made of an electrically insulating material (textolite), in which two diverters (2) are fixed. The diverters are similar to propellers with curved blades that can be right or left handed. The channel is fastened to a horizontal axle, rotated by an electric motor (5). A disk braking system (6) is fixed on the same axle. Initially, the fluid together with the toroidal channel is set in solid body rotation at a constant frequency which can be as high as 50 Hz. After braking, the vessel stops and, under the action of inertia, the diverters convert the toroidal motion of the fluid into a decaying turbulent screw flow (the flow decays in a few seconds, cf. Fig. 3 below).

The radius of the torus is $R=0.0875$ m, with a cross section of radius $r_0=0.0225$ m; the net mass of gallium is 5.58 kg. In practice, we have used a Ga-Zn-St alloy, made of 2% of Zn and 10.5% of St, with the advantage of a melting point at 19 °C. Its electrical conductivity is $\sigma=3.6\times10^6\ \Omega\,\mathrm{m}$ and its kinematic viscosity is $\nu=0.73\times10^{-6}\ \mathrm{m^2\,s^{-1}}$, both at room temperature. The rotation velocity of the channel was mainly 45 Hz as to avoid some mechanical resonances as well as to exclude coincidence with electrical current frequency. The accuracy of the angular velocity is equal to 0.5 Hz. The torus is halted in a braking time equal to 0.077 ± 0.005 s. The Reynolds number of the flow, based on the channel size and initial toroidal speed is $\mathrm{Re}=U_0 r_0/\nu=2\pi f R r_0/\nu$ is of the order of 10^6.

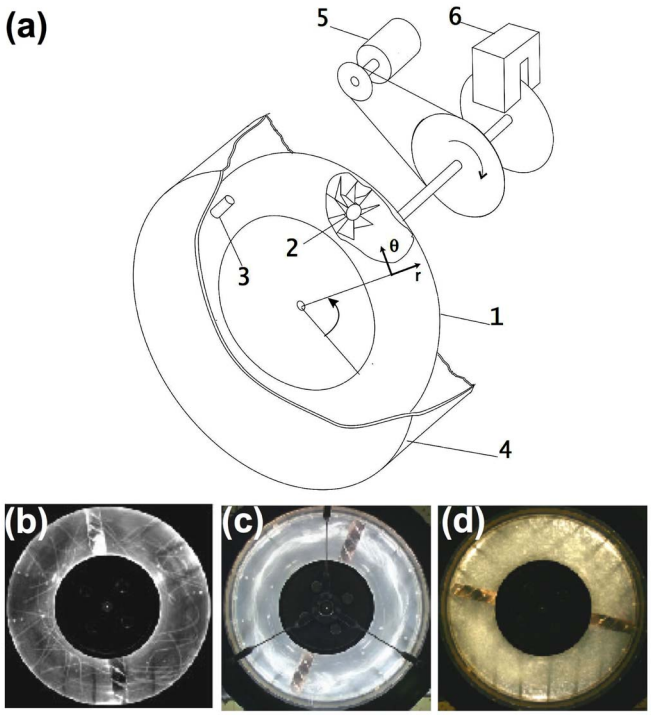

FIG. 1. (Color online) Principle of the Perm screw flow. (a) skematics of the experiments and components (1; toroidal channel, 2; diverter fixed in channel with left-hand or right-hand rotation, 3; magnetic sensor, 4; steel cover, 5; electromotor, 7; brake); (b) large scale flow vizualized by the trajectory of polystyrene particles (1–2 mm in diameter); (c) photograph of the screw flow in the torus seeded with air bubbles (illustration of the modes $m=3-5$); (d) small-scale structure of the screw flow in the torus, visualized by kalliroscope particles. The ratio R/r_0 is 3.89 for the gallium channel and 2.75 for the water channel, the corresponding Reynolds numbers are 1.3×10^6 and 1.4×10^6.

The properties of the flow were studied in experiments made in a similar model, filled with water [14,19]—in this case visualization and image processing allow to characterize the flow. The large scale flow velocity can be expressed as the sum of a toroidal component $[\mathbf{V}^T=V^T(r,z,t)\mathbf{e}_\theta$ along the axis of the torus] and a poloidal component $\mathbf{V}^P(r,z,t)$—the z axis is the axis of rotation of the channel. Reversing its direction of rotation changes the signs of both the poloidal and the toroidal velocity components, but keeps unchanged the sign of the large-scale helicity $H=\int_V \mathbf{V}\cdot(\nabla\times\mathbf{V})d^3r$. Replacing right diverters by left ones changes the sign of the poloidal component only, and thus reverses the sign of the large-scale helicity. The large scale helical motion is clearly seen in Fig. 1(b) showing the trajectory of advected—millimeter-sized—particles, while the small scale helical motion is evidenced in Fig. 1(d) where kalliroscope particles have been used.

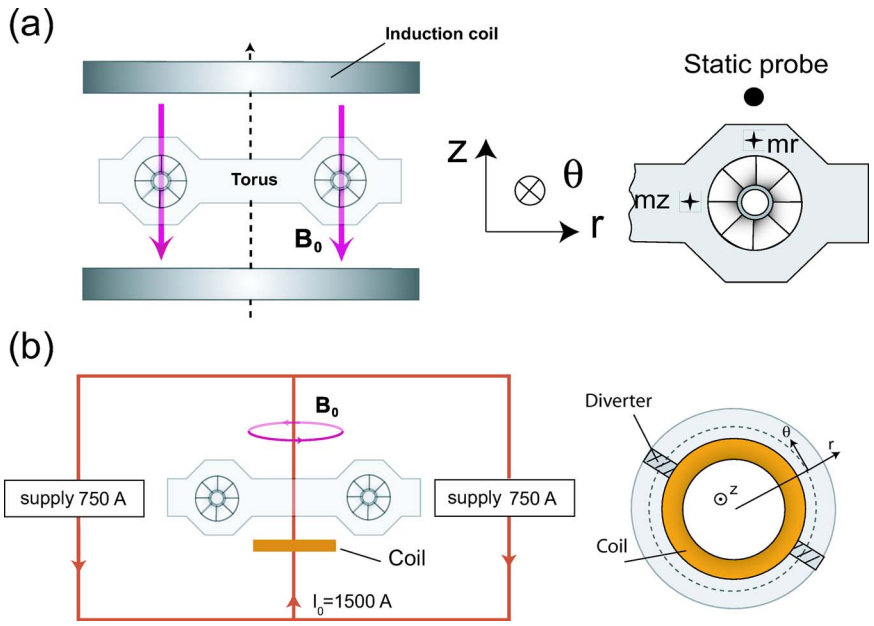

FIG. 2. (Color online) Magnetic induction measurements. (a) Case 1: the external magnetic field is applied transverse to the torus, $\mathbf{B}_0=B_0\mathbf{e}_z$, with $B_0=45$ G. The Hall probes are either stationary, enclosed in the steel casing (static probe), or moving with the torus at location mr and mz, 5 mm away from the channel. At location mr the probe is set to measure the radial field (along $\mathbf{e}_r$), while at location mz it measures the axial field (along $\mathbf{e}_z$). (b) Case 2: the external field is toroidal: the Fluxgate probes are set at locations ($r=8.7$ cm, $\theta=0$, $z=6.5$ cm) and ($r=8.7$ cm, $\theta=90°$, $z=6.5$ cm) where the applied field is respectively ($B_{0,r}=-1.2$ G, $B_{0,\theta}=27$ G, $B_{0,z}=3.9$ G) and ($B_{0,r}=3.6$ G, $B_{0,\theta}=33.5$ G, $B_{0,z}=-0.8$ G).

B. Induction measurements

In the experiment, an external magnetic field is applied by coils carrying electrical currents. Two main geometries are considered, as shown in Fig. 2:

(1) In the first case, a pair of Helmoltz-like coils are set on each side of the torus, in order to apply a field perpendicular to its axis, cf. Fig. 2(a). The coils have a radius ($R_C=17$ cm) larger than that of the channel. They are set 16 cm apart and are powered by dc batteries that deliver 25 A, so as to generate a 45 G homogeneous magnetic field. For security reasons the rotating channel is enclosed into a steel casing which has a weak magnetization. Its effect is subtracted in the computation of induction.

(2) In the second case, one wishes to apply a toroidal field, i.e., a field along the axis of the torus. In practice we use an electrical conductor carrying a strong current perpendicularly to the torus plane in its center. In order to minimize the contribution from the coils that connect the conductor to the power supply, two symmetric loops are formed as in Fig. 2(b). Two 750 A dc batteries are used; the conductor carrying the current through the axis of the torus is a 2 m long copper rod, while connectors to the batteries form a 3 m wide loop. The toroidal field inside the torus is equal to 35 G; because of the connections to the supply field is not exactly toroidal; there is a weak $m=1$ component (its peak amplitude is equal to 3 G).

Varying measurements of the magnetic fields induced by the flow motion have been made depending on the direction of the applied field:

(3) For a transverse field (applied along the z axis, case 1 above), Hall probes have been used. They are based on Sentron HSA-1M sensors, which have a sensitivity equal to 300 V/T across a 0–500 Hz dynamical range. Measurements have been made either in the laboratory reference frame, with probes fixed on the stationary steel casing, or in the torus reference frame with probes fixed on the textolite channel casing. In each case, the resolution of the measurement has proven to be limited by the output noise of the amplifiers included in the Hall sensors. It is equal to 0.01 G.

(4) For a toroidal applied field (case 2 above), the induced field proved to be much weaker and Fluxgate probes were used (model 503 from Applied Physics Systems), with a sensitivity equal to 4×10^4 V/T. The resolution of the measurement in this case is equal to 0.001 G. Since the flow is in free decay once the channel is halted, and hence nonstationary, global measurements can be made using an induction coil as shown in Fig. 2(b). Using amplification, we have been able to detect induced electromotive forces as low as 1 mV, corresponding to a 0.001 G magnetic field.

III. EXPERIMENTAL RESULTS

A. Response to a transverse field

Figure 3 shows local induction measurements at point 2, for a transverse field with amplitude 45 G. Measurements have been averaged over many runs (more than a dozen) and the fast fluctuations have been filtered out during signal processing. One thus expects to measure induction effects related to the large scale flow motion, as shown in Fig. 1(b). Before the channel is halted, the motion is a solid body rotation and no induction is expected (assuming a uniform applied field). Then, one observes a fast increase of the induc-

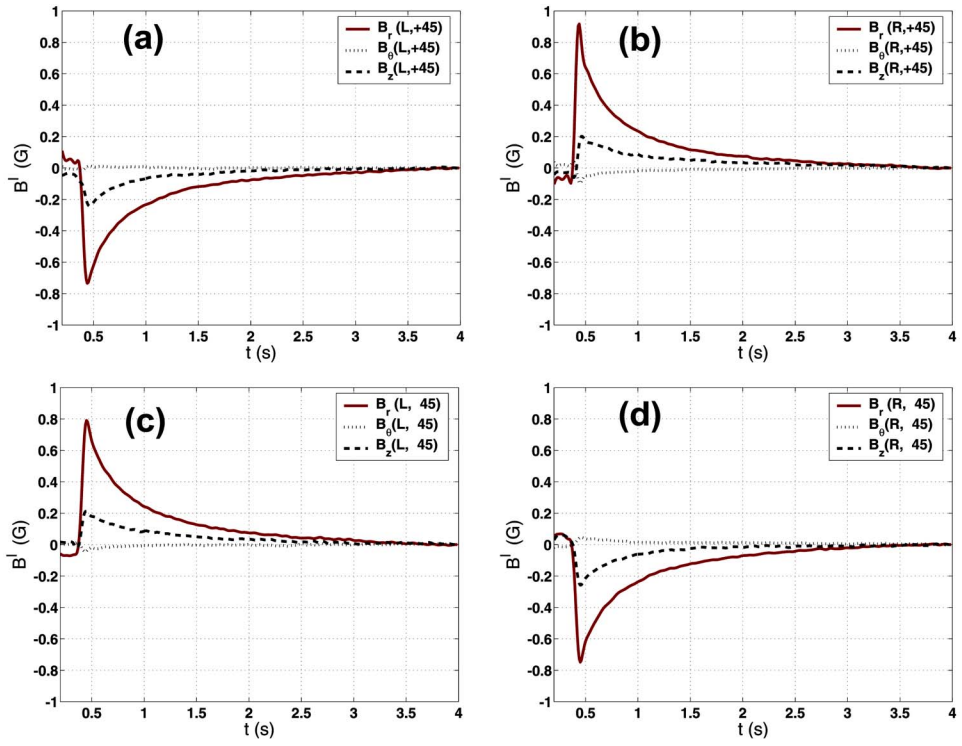

FIG. 3. (Color online) Transverse applied field, $\mathbf{B}_0=B_0\mathbf{e}_z$. Local measurement with a Hall probe located at position (2) (cf. Fig. 2). (left): channel equipped with left diverters, rotated in either direction [(a) and (c)]; (right): similar measurement for the channel equipped with right-handed diverters [(b) and (d)]. The experimental data have been low-pass filtered with a corner frequency equal to 40 Hz; many measurements are averaged.

tion as the channel stops ($t\in[0.3,0.4]$ s in the figure), and a slow decay as the screw flow loses its initial momentum ($t\in[0.5,4]$ s). A large induction is measured in the radial direction (B_r), with a smaller contribution in the axial direction (B_z) and a contributions in the azimuthal direction B_θ barely within the resolution of the measurement probe. In addition, (B_r,B_z) change sign when the initial rotation of the channel is reversed, or the right diverters replaced with left ones.

These features can be understood from a quasistatic analysis of the induction equation. We write it as

$$\partial_t\mathbf{B}=\nabla\times(\mathbf{V}\times\mathbf{B})+\lambda\Delta\mathbf{B}, \tag{2}$$

with the net magnetic field $\mathbf{B}$ expressed as the sum of the externally applied field $\mathbf{B}_0$ and of the induced field $\mathbf{B}^I$. As the screw flow decays, both the velocity and the magnetic fields are functions of time, but one notes that the magnetic diffusion time $\tau_M=r_0^2/\lambda\sim 2.5$ ms is much smaller than the characteristic time of decay of the flow (of the order of 1 s). As a result, the induction equation may be approximated by

$$\mathbf{0}=\nabla\times[\mathbf{V}(t)\times(\mathbf{B}_0+\mathbf{B}^I(t)\ ]+\lambda\Delta\mathbf{B}^I(t). \tag{3}$$

For further analysis, the velocity is split into poloidal and toroidal components

$$\mathbf{V}(r,z,t)=\mathbf{V}^T(r,z,t)+\mathbf{V}^P(r,z,t)=V^T(r,z,t)\mathbf{e}_\theta+\{V_r^P(r,z,t)\mathbf{e}_r+V_z^P(r,z,t)\mathbf{e}_z\}, \tag{4}$$

which change with direction of rotation or inversion of the diverters as shown in Table I. Now, for a field applied in the transverse direction, $\mathbf{B}_0=B_0\mathbf{e}_z$, and in a first order linear approximation, one has

$$\lambda\Delta\mathbf{B}^I(t)+B_0\partial_z\mathbf{V}(t)=\mathbf{0}. \tag{5}$$

One thus expects that the poloidal flow component deforms the applied field as shown in Fig. 4(a). The drawings corresponds to a situation with right diverters and a positive value of the initial rotation of the channel, i.e., as in Fig. 3(b). A positive magnetic field is induced in the radial direction, together with a stretching of the imposed field line which corresponds to a positive field also induced in the axial z direction. The evolution of the figures, from 3(a)–3(d) is in agreement with the above description and the symmetries of the flow shown in Table I. For instance, when the initial rotation of the channel is reversed for identical diverters, one changes the signs of both the poloidal and the toroidal velocities and one sees in Figs. 3(a)–3(d) that the sign of the induced magnetic fields is also reversed. This is in agreement with a linear (first order) induction process (with respect to the magnetic Reynolds number) as supposed in order to es-

TABLE I. Symmetries of the large scale flow, with respect to changes in the initial direction of rotation of the channel and diverter shape.

Direction of rotation	Diverter	Flow	Helicity
$f>0$	Right	$\mathbf{V}^P+\mathbf{V}^T$	$H>0$
$f<0$	Right	$-\mathbf{V}^P-\mathbf{V}^T$	$H>0$
$f>0$	None	$\mathbf{V}^T$	$H=0$
$f<0$	None	$-\mathbf{V}^T$	$H=0$
$f>0$	Left	$-\mathbf{V}^P+\mathbf{V}^T$	$H<0$
$f<0$	Left	$\mathbf{V}^P-\mathbf{V}^T$	$H<0$

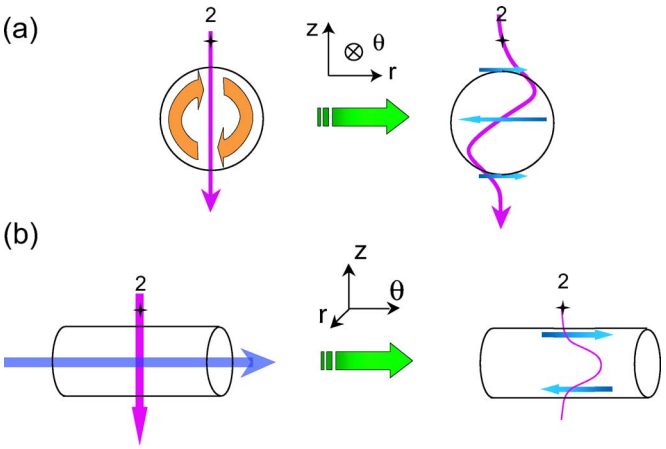

FIG. 4. (Color online) Transverse applied field, $\mathbf{B}_0 = B_0 \mathbf{e}_z$. Schematics of the induction created by advection of the applied field lines: (a) action of the poloidal velocity component; (b) action of the toroidal velocity component. The drawings corresponds to the situation with right diverters and a positive value of the initial rotation of the channel.

tablish Eqs. (5). The toroidal induction generated by the toroidal velocity, sketched in Fig. 4(b), is limited to the bulk of the fluid flow. It cannot be measured in the insulating region outside of the flow. In fact this result is valid for any contribution to the induction that involves the toroidal flow component, see the Appendix for a proof. For instance, this is the case of the Parker effect [12]. It has been evidenced in swirling flows of sodium [9] and gallium [17] using Hall probes located inside the flow, but it cannot be accessed here by probes located outside of the channel.

However nonlinear effects in the induction are expected in the measurements, and indeed observed. This is the case of the expulsion of the applied transverse field lines by the poloidal flow component. The mechanism is detailed in Fig. 5. The poloidal flow motion first deforms the applied field lines by the linear mechanism described above, Fig. 5(a). This generates an induced component $\mathbf{B}_1^I$ which solves $\lambda \Delta \mathbf{B}_1^I + B_0 \partial_z \mathbf{V}^P = \mathbf{0}$. This induced field is in turn acted upon by the poloidal velocity to generate an induced field $\mathbf{B}_2^I$, solution of $\lambda \Delta \mathbf{B}_2^I + \nabla \times (\mathbf{V}^P \times \mathbf{B}_1^I) = \mathbf{0}$. As a result a magnetic field component opposed to the applied field is induced in the center of the channel, while the field on the sides is increased, Fig. 5(b). This effect corresponds to the expulsion of the applied field from the eddy motion of the poloidal velocity [20–23]. It is shown in Fig. 5(c): as the magnetic Reynolds number increases the axial B_z component at location mz increases then saturates as the applied field is expelled. The effect is quadratic and thus even with respect to a change in the initial direction of rotation of the channel, i.e., as $\mathbf{V}^P$ is changed into $-\mathbf{V}^P$ (Table I). At the largest initial speed of the channel ($f \sim 45$ Hz) one measures at location mz an induced field equal to 0.3 G (for a 45 G applied field).

B. Response to a toroidal field

We consider here the measurements made with an applied toroidal field, generated by a strong current (~ 1000 A) flowing along the z axis. We concentrate on the possibility of induction of a toroidal current. As we shall see the induction is small, and local measurements would be further perturbed by the finite extension of the cables connecting the conductor on the z axis to the power supply [cf. Fig. 2(b) right]. We have thus made a global measurement with an induction coil whose axis is aligned with that of the torus [cf. Fig. 2(b) left]. Such a measurement is meaningful because the flow is decaying so that the magnetic flux across the induction is not stationary. When the coil is connected to a voltage amplifier with gain G, the output can be expressed as

$$U(t) = -NSG\frac{d\bar{B}_z}{dt} \quad \text{with} \quad \bar{B}_z = \frac{1}{S}\int_S B_z(t)dS, \qquad (6)$$

defined as the average z component of the magnetic field across the coil area S (N is the number of windings).

The measurements are shown in Figs. 6(a)–6(c). There, the initial rotation rate of the channel is fixed to 45 Hz in either direction, and one compares measurements obtained with left 6(a) or right 6(c) diverters and also without diverters 6(b). The curves are an average of 10 measurements, with $t=0$ defined as the onset of breaking. In the early stage $t < 0.2$ s, the recorded variations are due to the electromagnets that control the brakes; they are also detected when the diverters are removed and thus are unrelated to the screw

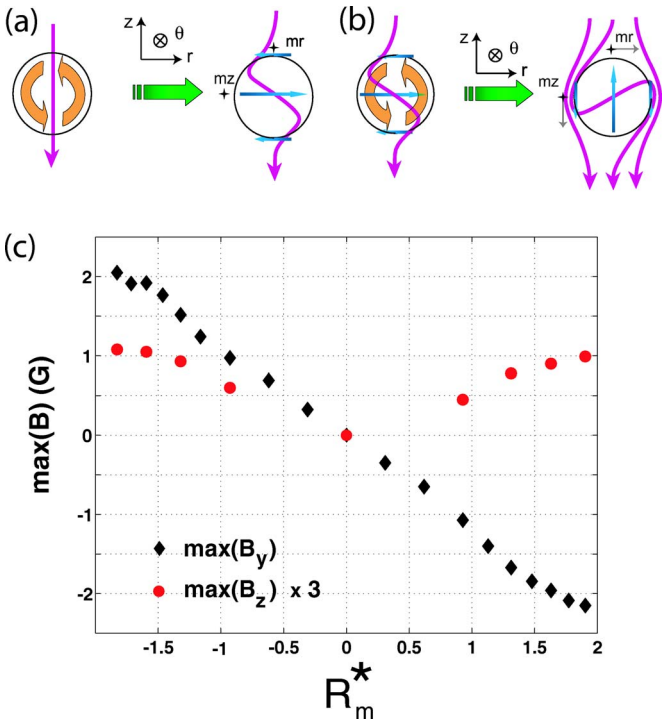

FIG. 5. (Color online) Nonlinear expulsion effect, transverse applied field. (a) and (b) sketch of the mechanism of expulsion of the applied field lines; (c) measurements of the maximum of the radial induced field B_r at location mr (diamonds) and of the maximum of the axial induced field B_z at location mz. The magnetic Reynolds number has been corrected to include the slight variation of the braking time of the channel as its initial speed increases. The applied field is $B_{0,z} = 45$ G.

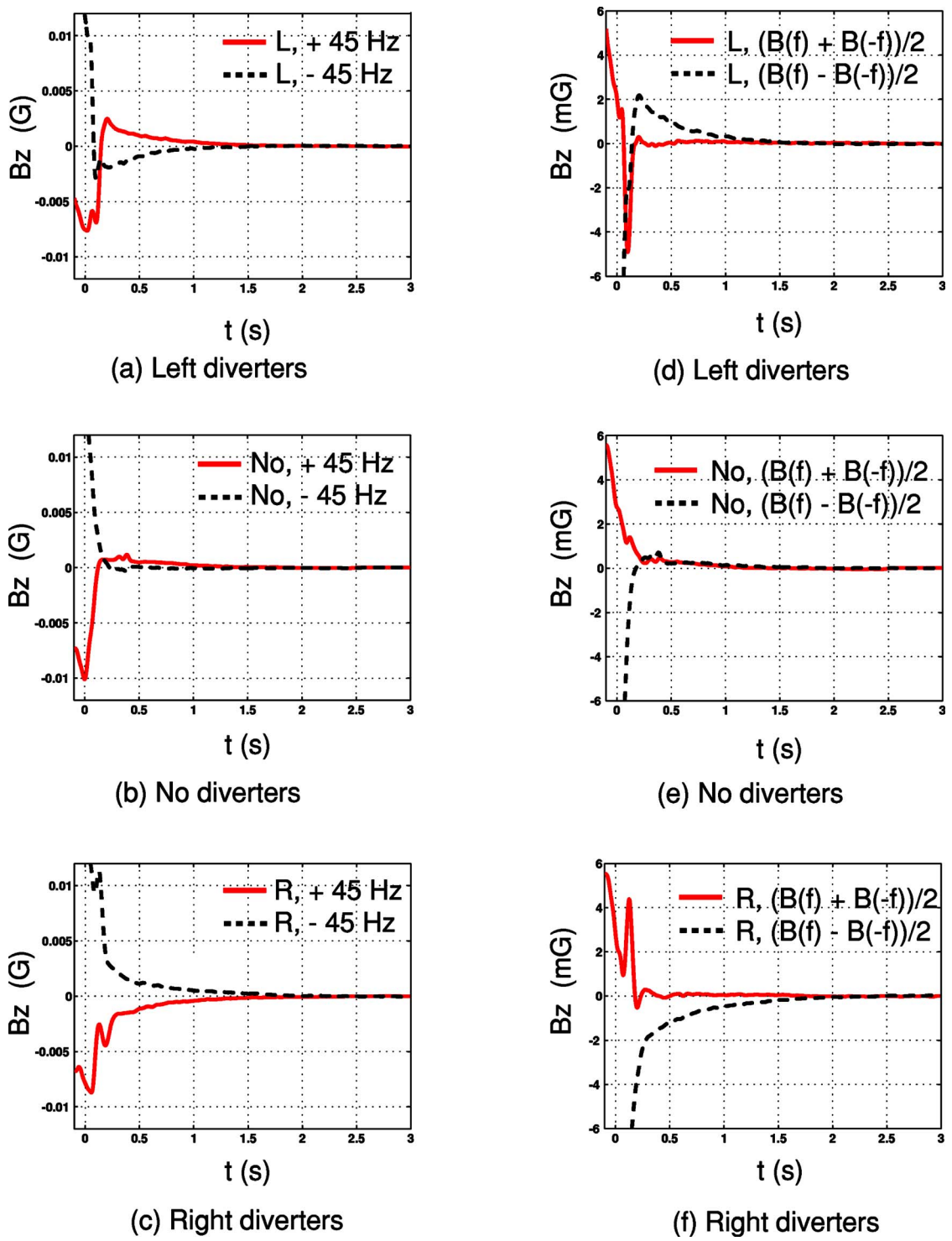

FIG. 6. (Color online) Applied toroidal field, $\mathbf{B}_0=35$ G. Measurement using an induction coil, as shown in Fig. 2(b): the data corresponds to the average field $\bar{B}_z(t)$ across the coil. (left): raw data for positive and negative rotation rates; (right): corresponding odd and even parts.

motion. At later stages, one observes two type of behavior: a slow decrease that change its sign when either the diverters are exchanged or the channel rotated in the opposite direction (thus having the symmetry of the poloidal flow $\mathbf{V}^P$) and a localized peak [see 6(c)] just after the channel has stopped.

The above features are more apparent when the induction is split into contributions that are odd and even with respect to the initial rotation, $(1/2)[\bar{B}_z(f) \pm \bar{B}_z(-f)]$. The curves are shown in Figs. 6(d)–6(f). The odd part has the symmetry of $\mathbf{V}^P$ and decays with the large scale flow. It has in fact the same characteristics as would result from a transverse applied field. Its amplitude, 2 mG, is consistent with the slight asymmetry in the cables that connect the rod generating the applied field to the power supply. Indeed for an applied

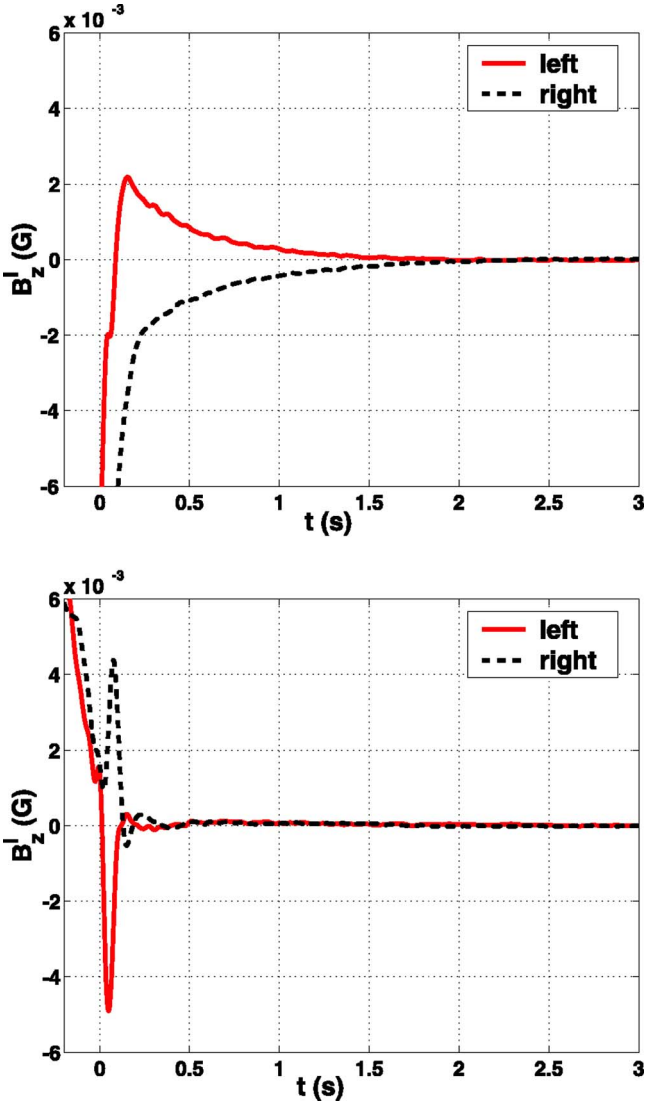

FIG. 7. (Color online) Applied toroidal field, $\mathbf{B}_0=35$ G. Odd (a) and even (b) parts of the measurement with the induction coil. The data corresponds to Figs. 6(d) and 6(f).

transverse field with amplitude 40 G, we have measured a 0.2 G induction; a 2 mG effect is consistent with a 0.5 G imbalance in the cable layout. The even contribution [solid lines in 6(d) and 6(f)] has a maximum amplitude equal to 5 mG and lasts for about 50 ms as the channel is stopped. This effect changes its sign when left diverters are replaced with right ones. These observations are summarized in Fig. 7: the odd and slowly decaying part of the induction is attributed to the existence of a small spurious transverse field, while the even peak has the symmetry of the flow helicity. We note that there is no detectable contribution with even parity during the slow decay of the large scales motion, i.e., for times between 0.3 and 2 s.

IV. DISCUSSION

In this section we analyze further our measurements, with particular focus on the relationship between induction and helicity. Concerning our measurements for an applied axial field $B_{0,z}$, a first observation is that we have not been able to measure directly the Parker effect expected from the flow screw motion. This is due to the fact that the probes were located *outside* of the flow, in the external insulating medium where the induction from the toroidal flow is out of reach, Appendix. However the expulsion of the field lines (a twin mechanism of the Parker effect [9,17]) has been observed, Sec. III A, with its nonlinear evolution. This is important because is shows that nonlinear induction mechanisms do occur and can be detected in the experiment.

A. Parker effect, case of an applied toroidal field

A first nonlinear induction mechanism that could be expected, comes from the large scale screw motion when the applied field is toroidal. Of course, no effect should occur when the flow helicity is everywhere aligned with the applied field $\mathbf{B}_0=B_0\mathbf{e}_\theta$, but visualizations, such as in Fig. 1(c), indicate that the large scale motion is not always invariant in the azimuthal direction. Spiralling motion with azimuthal modes $m=3$ and $m=5$ have been observed. In this case, there is an angle between the applied field and the helical field lines, and a large scale Parker effect may be expected. It can be estimated using (i) the data from the expulsion effect and (ii) the measurements in the von Kármán setup [17] where the expulsion and the Parker effect have been measured simultaneously. The upper value of 300 mG obtained for the expulsion (Fig. 5) correspond to maximum values for a toroidal Parker effect between 20 and 30 mG for azimuthal helical modes between $m=3$ and $m=5$. This induced component should decay slowly with the large scale flow. Both features (an amplitude of the order of 10 mG and a slow decay in time) are not observed in our measurement [Fig. 7(b)] although our 1 mG resolution would be sufficient.

B. Alpha effect, toroidal applied field

We consider here the alpha effect, that is the possibility that cooperative effects may arise from the induction at small scales and contribute to the large scale magnetic field. This is best analyzed in the framework of the mean-field theory, which we briefly recall and use to estimate the order of magnitude of such a contribution.

We recall that here turbulence arises in the toroidal flow through the instability of an initially (quasi) laminar screw flow, with helicity initially confined in the large scales. The development of helical small scales is attributed to a cascade of helicity. There are arguments for such an helicity cascade, at least in periodic domains [15]. Visualization using reflecting anistropic particles [kalliroscope, Fig. 1(d)] also support this idea. We stress that we have no definite argument for this (because small scale helicity measurements are impossible in the rotating channel), but taking into account that the large-scale flow is very much helical (the dimensionless helicity is of order of unity) one can hardly suppose that no helicity is transported in smaller scales.

1. Some theoretical background from mean-field electrodynamics

Let us consider a locally *cylindrical* mean screw flow (uniform along the cylinder) with turbulent small scales. The

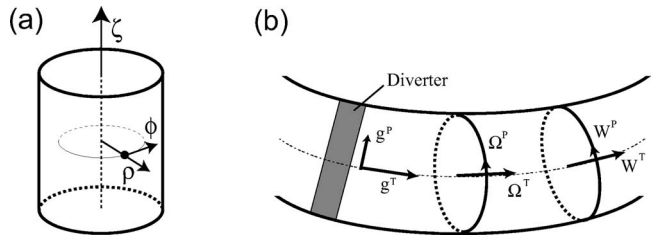

FIG. 8. Contribution from inhomgeneities. (a) Local cylindrical coordinates; (b) orientations of the vectors $\boldsymbol{g}$, $\boldsymbol{W}$, $\boldsymbol{\Omega}$ which enter in the mean electromotive force [Eqs. (8)].

cylindrical coordinates are (ρ,ϕ,ζ) and the velocity is expressed as $\mathbf{V}=\bar{\boldsymbol{U}}+\mathbf{u}$ with $\bar{\boldsymbol{U}}$ the mean flow and $\mathbf{u}$ its turbulent fluctuations, cf. Fig. 8. This approximations discards curvature effects, but in the experiment they would be of the quadratic in the torus aspect ratio $r_0/R=0.26$, leading to corrections of the order of 7% [24]. Calculations assuming a cylindrical geometry will thus provide a useful first order estimation.

If the turbulence is homogeneous (but devoid of mirror symmetry), then the alpha terms in the mean electromotive force due to the small scale motions can be written [13] as

$$\boldsymbol{\mathcal{E}}^{(0)}=-\alpha_0^{(H)}\bar{\boldsymbol{B}}-\alpha_0^{(D)}\boldsymbol{D}\cdot\bar{\boldsymbol{B}}, \tag{7}$$

where H is the flow helicity and $\boldsymbol{D}$ is the symmetric part of the gradient tensor of $\bar{\boldsymbol{U}}$, $D_{ij}=\frac{1}{2}(\partial\bar{U}_i/\partial x_j+\partial\bar{U}_j/\partial x_i)$, related to the large scale shear. For turbulent flows, and under a first-order smoothing approximation (justified here because the magnetic Reynolds number is at best of the order of unity), the magnitude of α can be estimated as [2]

$$\alpha_0^{(H)}=\frac{-1}{3\lambda}\int k^{-2}F(k)dk, \tag{8}$$

where $F(k)$ is the helicity spectrum.

If the small scale motions deviate from homogeneity through the existence of a gradient of turbulence intensity $\boldsymbol{g}=(1/\overline{u^2})\boldsymbol{\nabla}\overline{u^2}$, then terms must be added to the above expression. The most general form for the additional α terms in the electromotive force $\boldsymbol{\mathcal{E}}$ is [23,24]

$$\begin{aligned}\boldsymbol{\mathcal{E}}^{(1)}=&-\alpha^{(D)}\tilde{\alpha}(\boldsymbol{g},\boldsymbol{D})\cdot\bar{\boldsymbol{B}}-\alpha_1^{(\Omega)}(\boldsymbol{g}\cdot\boldsymbol{\Omega})\bar{\boldsymbol{B}}\\&-\alpha_2^{(\Omega)}[(\boldsymbol{\Omega}\cdot\bar{\boldsymbol{B}})\boldsymbol{g}+(\boldsymbol{g}\cdot\bar{\boldsymbol{B}})\boldsymbol{\Omega}]-\alpha_1^{(W)}(\boldsymbol{g}\cdot\boldsymbol{W})\bar{\boldsymbol{B}}\\&-\alpha_2^{(W)}[(\boldsymbol{W}\cdot\bar{\boldsymbol{B}})\boldsymbol{g}+(\boldsymbol{g}\cdot\bar{\boldsymbol{B}})\boldsymbol{W}],\end{aligned} \tag{9}$$

where $\hat{\alpha}_{ij}=(\epsilon_{ilm}D_{lj}+\epsilon_{jlm}D_{li})g_m$. The mean flow is wrtitten as $\bar{\boldsymbol{U}}=(0,\rho\Omega(\rho),\bar{U}_\zeta(\rho,\zeta))$ in cylindrical coordinates and $\boldsymbol{W}$ stands for $\boldsymbol{\nabla}\times\bar{\boldsymbol{U}}$, see Fig. 8 for the orientations of these vectors. As usual in mean-field magnetohydrodynamics, not too large variations of mean quantities like $\bar{\boldsymbol{U}}$, $\overline{u^2}$, and $\bar{\boldsymbol{B}}$ in space and time have been assumed. For the sake of simplicity it has been further assumed that the influence of the Coriolis force and the mean motion on the turbulence is sufficiently weak so that $\boldsymbol{\mathcal{E}}$ is linear in both $\boldsymbol{\Omega}$ and the derivatives of $\bar{\boldsymbol{U}}$, that is in $\boldsymbol{W}$ and $\boldsymbol{D}$. Any influence of the magnetic field on the motion has been ignored. The coefficients $\alpha_1^{(\Omega)},\alpha_2^{(\Omega)},\ldots$ are determined by the small scale features of $\mathbf{u}$ and are independent of $\boldsymbol{\Omega}$, $\boldsymbol{W}$, $\boldsymbol{D}$, and $\bar{\boldsymbol{B}}$.

2. Estimations and comparison with measurements

The theoretical argument given in the previous subsection confine the possible mechanism of generation of electromotive force directed along the axis of the channel by a *stationary*, *ζ-independent* flow. Let us remember that the axis ζ of cylindrical coordinate system follows the channel direction and corresponds to the azimuthal coordinate in the torus. Only intrinsically helical turbulence contributes to the alpha effect.

The measurements reported in Sec. III B yield a maximum values of $\bar{B}_z=5\pm0.5$ mG for the zero azimuthal mode of poloidal magnetic field having the symmetry of the flow helicity. In time, this amplitude is sharply peaked immediately after the toroidal channel is stopped. The measured value of the induced field can be linked to the alpha coefficient using Ampere's law

$$\bar{B}_z=\frac{\alpha\pi r_0^2}{2\lambda R}B_0\Rightarrow[\alpha]\approx\frac{2\lambda R}{\pi r_0^2}\frac{\bar{B}_z}{B_0}\sim(3\pm0.3)\times10^{-3}\ \mathrm{m/s}. \tag{10}$$

After this phase, the induction component with the symmetry of the helicity drop to values $\bar{B}_z<0.1$ mG (cf. Fig. 7), corresponding to $\alpha<0.6\times10^{-4}$ m/s.

We now compare these observations to estimations from mean field theory. A contribution from the small scale turbulence can be estimated using Eqs. (8). One obtains [2]

$$\alpha\approx u_{\mathrm{rms}}\mathrm{R_m}, \tag{11}$$

where u_{rms} is the root-mean-squared intensity of velocity fluctuations. Hydrodynamic measurements in a water prototype of the experiment have shown that u_{rms} is of the order of 10% of the rotation speed of the channel $\bar{U}=2\pi Rf$ before it is halted. With typical values $\bar{U}\sim10$ m/s in the experiment, one obtains $\alpha\sim0.1$ $\mathrm{R_m}$. Using for $\mathrm{R_m}$ the integral value, of the order of unity in the experiment, one gets $\alpha\sim0.1$ m/s, much larger than observed. One may argue [21] that a more meaningful estimation of the magnetic Reynolds number is provided at low $\mathrm{R_m}$ by the ratio of the maximum induced field to the applied one, in which case on gets an *intrinsic* magnetic Reynolds number of the order of 0.1 for the experiment. This still yields an estimation of $\alpha\sim0.01$ m/s, still much larger than the measured value.

In fact, the sharply peaked behavior observed in Fig. 7 can only be generated in the time period where the screw motion is established. When channel stops, the fluid passes through the diverters and an initial screw motion is propagated along the toroidal channel. For the measurement in Fig. 7, the duration of the induction peak corresponds to about 4 rotations of the fluid along the channel length. During this phase, the flow is inhomogeneous in the azimuthal direction, both in regards to its mean $\bar{\boldsymbol{U}}=(0,\rho\Omega(\rho,\zeta),\bar{U}_\zeta(\rho))$ and to its small scale fluctuations. As

long as the applied field B_0 is axisymmetric, the large inhomogeneity in the large scale is not expected to contribute to the *integrated* induction $\bar{B}_z$. The small scale fluctuations may contribute, according to the expression in Eqs. (8). The gradient $\boldsymbol{g}$ may develop a toroidal component $\boldsymbol{g}^T$ (along the channel, cf. Fig. 8) and a poloidal one $\boldsymbol{g}^P$ (in the ρ direction). Restricting ourselves to the generation of an electromotive force in the direction of $\bar{\boldsymbol{B}}$ (along the ζ axis), we see in Eqs. (8) that $\boldsymbol{g}^P$ does not contribute since it is perpendicular to $\boldsymbol{\Omega}$, $\boldsymbol{W}$, and $\bar{\boldsymbol{B}}$; in addition the $\hat{\alpha}(\boldsymbol{g},\boldsymbol{D})$ yields a zero contribution [24] because it has no diagonal component. So contributions to $\boldsymbol{\mathcal{E}}_\zeta$ are due to the gradient $\boldsymbol{g}^T$ and can be rewritten, from (8) under the form

$$\boldsymbol{\mathcal{E}}_\zeta = \alpha^{(\omega,W)} g^T (W_\zeta \text{ or } \Omega_\zeta)\bar{B}, \tag{12}$$

with a coefficients $\alpha^{(\omega,W)}$ computed in [24] and whose order of magnitude for liquid metals at low magnetic Reynolds number as

$$\alpha^{(\omega,W)} \sim \frac{1}{10} \mathrm{R_m}^2 r_0^2. \tag{13}$$

We first note here that $\mathcal{E}_\zeta$ in Eqs. (11) has the symmetry of the flow helicity, since (W_ζ, Ω_ζ) transform as $\mathbf{V}^P$ and $\boldsymbol{g}^T$ transforms as $\mathbf{V}^T$. So this term is a possible candidate for the generation of the induction peak observed in Fig. 7, as it has the right symmetries and a finite life time (the time of establishment of the screw flow inside the halted torus). Numerically, one can estimate $g^T \sim R$ and $W_\zeta \sim \Omega_\zeta \sim f$, so that one finds $\boldsymbol{\mathcal{E}}_\zeta/\bar{B} \sim 0.1$ if the integral Reynolds number is used in $\mathrm{R_m}$, or $\boldsymbol{\mathcal{E}}_\zeta/\bar{B} \sim 0.001$ using the intrinsic one. In the later case the resulting value is of the order of magnitude of the measurement for the induction peak in Fig. 7.

C. Concluding remarks

Our measurements give an upper bound for the contribution of helical turbulence to the magnetic induction at large scales. We find that α is less than 10^{-4} m/s in the homogeneous decay and that α is of the order of 10^{-3} when a gradient of turbulence travels along the channel. Compared to the initial large scale flow velocity $\bar{U} = 2\pi R f$, it corresponds to $\alpha/\bar{U} \sim 10^{-5}$ and $\alpha/\bar{U} \sim 10^{-4}$, respectively. It is interesting to evaluate how these measurement extrapolate to flows of larger size using liquid sodium instead of gallium, because such configurations are currently investigated for the generation of laboratory dynamos. Using Eqs. (10), one estimates

$$\frac{\alpha(\mathrm{Na})}{\alpha(\mathrm{Ga})} \sim \frac{L(\mathrm{Na})}{L(\mathrm{Ga})} \frac{\mathrm{R_m(Na)}}{\mathrm{R_m(Ga)}}, \tag{14}$$

where L and $\mathrm{R_m}$ are the respective size and magnetic Reynolds number of the experiments (compared for a given geometry). In practice sodium experiments with a 1 meter characteristic size are operated, and they reach magnetic Reynolds number up to 50. The above scaling implies that the alpha coefficient can grow a factor of 500 larger, corresponding to $\alpha_{\max} \sim 10$ cm/s. This "velocity" is still very much lower than the large scale speeds, so that in a sodium experiment one would still have $\alpha/\bar{U}$ limited to 10^{-3} to 10^{-2}. However, these estimates have been derived using a first order smoothing approximation. Possible improving correction may come from the fact that at larger $\mathrm{R_m}$ Eqs. (10) should read $\alpha = u_{\mathrm{rms}} \mathcal{F}(\mathrm{R_m})$ where $\mathcal{F}$ is a nonlinear function of the magnetic Reynolds number. Measurements in actual sodium experiments should be available in the near future.

Finally we note that the flow turbulence may induce other components to the effective electromotive force $\boldsymbol{\mathcal{E}}$ [13,23,24]. A contribution $\gamma \times \bar{\boldsymbol{B}}$, the gamma effect, would contribute to the expulsion of the applied magnetic field lines, and a contribution $\beta \boldsymbol{\nabla} \times \bar{\boldsymbol{B}}$ to enhanced magnetic diffusion. In our experiment these terms lead to corrections to the induction by the mean flow. Their detection needs specific measurements, some of them being currently under way.

ACKNOWLEDGMENTS

We aknowledge many useful discussions with Cary Forest, Philippe Odier, Woodrow Shew, Andrey Sukhanovsky, and Stanislas Kripchenko. This work was funded by ISTC under Project No. 2021, and by the ECONET program 10257QL.

APPENDIX

We first show that an induced toroidal field $\mathbf{B}^T$ cannot be measured in the insulating material surrounding the fluid. Indeed, the currents must vanish in the insulator, corresponding to $\boldsymbol{\nabla} \times \mathbf{B}^T = \mathbf{0}$. In cylindrical polar coordinates, this corresponds to

$$-\partial_z B^T(r,z)\mathbf{e}_\theta + \frac{1}{r}\partial_r [r B^T(r,z)] = 0.$$

This condition is met either when B^T is identically null, or when it is constant in the z direction and varies radially as $1/r$. This later solution corresponds to a field generated by a current in an infinitely long wire the along the z axis. It does not met the requirement that $\mathbf{B}$ should vanish at infinity.

We then proceed to show that induction effects due to the poloidal velocity component cannot be measured in the insulating region outside the flow. In order to do this, we compute the induction term as

$$\begin{aligned}\boldsymbol{\nabla} \times (\mathbf{V} \times \mathbf{B}) = {} & \boldsymbol{\nabla} \times (\mathbf{V}^T \times \mathbf{B}^T) + \boldsymbol{\nabla} \times (\mathbf{V}^P \times \mathbf{B}^P) \\ & + \boldsymbol{\nabla} \times (\mathbf{V}^T \times \mathbf{B}^P) + \boldsymbol{\nabla} \times (\mathbf{V}^P \times \mathbf{B}^T).\end{aligned}$$

The first term vanishes because $\mathbf{V}^T$ and $\mathbf{B}^T$ are parallel. The second term corresponds to the expulsion effect described in Sec. III A. The third and fourth term mix the poloidal and toroidal field. It is easy to show that they induce a toroidal field. Indeed

$$\boldsymbol{\nabla} \times (\mathbf{V}^P \times \mathbf{B}^T) = \{(\mathbf{V}^P \cdot \boldsymbol{\nabla}) B^T\}\mathbf{e}_\theta - \frac{B^T V_r^P}{r}\mathbf{e}_\theta,$$

directed along the azimuthal direction. The resulting toroidial field cannot be measured inside the insulating surroundings, as pointed out previously. The argument is analogous for the $\boldsymbol{\nabla} \times (\mathbf{V}^T \times \mathbf{B}^P)$ term.

[1] P. Roberts, *Magnetohydrodynamics and the Earth's Core* (Fluid Mechanics of Astrophysics and Geophysics, Vol. 10), edited by A. Soward and X. Andrew, (Taylor & Francis, 2002).
[2] H. K. Moffatt, *Magnetic Field Generation in Electrically Conducting Fluids* (Cambridge University Press, Cambridge, 1978).
[3] G. Chabrier and M. Küker, Astron. Astrophys. **446**, 1027 (2006).
[4] F. H. Busse, E. Grote, and A. Tilgner, Stud. Geophys. Geod. **42**, 211–223 (1998).
[5] E. Dormy, J.-P. Valet, and V. Courtillot, Geochem., Geophys., Geosyst. **1**, 62 (2000).
[6] B. Lehnert, Ark. Fys. **13**, 109 (1957).
[7] M. Steenbeck, I. M. Kirko, A. Gailitis, A. P. Klyavinya, F. Krause, I. Ya. Laumanis, and O. A. Lielausis, Sov. Phys. Dokl. **13**, 443 (1968).
[8] A. Gailitis *et al.*, Phys. Rev. Lett. **84**, 4365–4368 (2000).
[9] F. Pétrélis, L. Marié, M. Bourgoin, A. Chiffaudel, F. Daviaud, S. Fauve, P. Odier, and J.-F. Pinton, Phys. Rev. Lett. **90**(17), 174501 (2003).
[10] U. Muller, R. Stieglitz, and S. Horany, J. Fluid Mech. **498**, 31 (2004).
[11] A. Tilgner, Phys. Fluids **14**, 4092 (2002).
[12] E. N. Parker, Astrophys. J. **122**, 293 (1955).
[13] F. Krause and K.-H. Rädler, *Mean field Magnetohydrodynamics and Dynamo Theory* (Pergamon Press, New York, 1980).
[14] P. Frick, V. Noskov, S. Denisov, S. Khripchenko, D. Sokoloff, R. Stepanov, and A. Sukhanovsky, Magnetohydrodynamics **38**, 136 (2002).
[15] Q. Chen, S. Chen, and G. Eyink, Phys. Fluids **15**, 361 (2002); Q. Chen, S. Chen, G. Eyink, and D. Holm, Phys. Rev. Lett. **90**, 214503 (2003).
[16] Helicity is not stricly required. Parker or alpha effects would be engineered from flows in which the rotational and axial motions are disjoined, but when magnetic diffusivity is taken into account this is equivalent to helical motion.
[17] M. Bourgoin, R. Volk, P. Frick, S. Kripchenko, P. Odier, and J.-F. Pinton, Magnetohydrodynamics **1**, 13 (2004).
[18] Louis Marié, Ph.D. Université Paris 7, (2003); [http://tel.ccsd.cnrs.fr/documents/archives0/00/00/77/55/index.html]; M. Bourgoin, Ph.D. (École Normale Supérieure de Lyon, 2003); [http://tel.ccsd.cnrs.fr/documents/archives0/00/00/83/02/index.html] R. Volk, Ph.D. (École Normale Supérieure de Lyon, 2005).[http://tel.ccsd.cnrs.fr/tel-00011221/en/]
[19] S. Denisov, V. Noskov, A. Sukhanovskiy, and P. Frick, Fluid Dyn. **36**, 734 (2001).
[20] N. O. Weiss, Proc. R. Soc. London **A293**, 310 (1966).
[21] A. Martin, P. Odier, J.-F. Pinton, and S. Fauve, Eur. Phys. J. B **18**, 337 (2000).
[22] V. Noskov, S. Denisov, P. Frick, S. Khripchenko, D. Sokoloff, and R. Stepanov, Eur. Phys. J. B **41**, 561 (2004).
[23] R. Stepanov, Ph.D. Thesis (ICMM, Perm, 2000).
[24] K.-H. Rädler and R. Stepanov, Phys. Rev. E (unpublished).